Carbohydrate Polymers 175 (2017) 689–698

Contents lists available at ScienceDirect

Carbohydrate Polymers

journal homepage: www.elsevier.com/locate/carbpol

Research Paper

Chitosan composite hydrogels reinforced with natural clay nanotubes

Biao Huang, Mingxian Liu*, Changren Zhou

Department of Materials Science and Engineering, Jinan University, Guangzhou 510632, China

ARTICLE INFO

Keywords:
Halloysite
Chitosan
Hydrogels
Composite
Biocompatibility
Doxorubicin

ABSTRACT

Here, chitosan composites hydrogels were prepared by addition of halloysite nanotubes (HNTs) in the chitosan KOH/LiOH/urea solution. The raw chitosan and chitosan/HNTs composite hydrogels were obtained by heat treatment at 60 °C for 8 h and then regeneration in ethanol solution. The viscosity of the composite solution is increased with HNTs content. The Fourier transform infrared spectroscopy (FT-IR) shows that the hydrogen bonds interactions exist between the HNTs and the chitosan. X-ray diffraction (XRD) results show that the crystal structure of HNT is not changed in the composite hydrogels. The compressive property test and storage modulus determination show that the mechanical properties and anti-deformation ability of the composite hydrogel significantly increase owing to the reinforcing effect of HNTs. The composites hydrogel with 66.7% HNTs can undergo 7 times compression cycles without breaking with compressive strength of 0.71 MPa at 70% deformation, while pure chitosan hydrogel is broken after bearing 5 compression cycles with compressive strength of 0.14 MPa and a maximum deformation of 59%. A porous structure with pore size of 100–500 μm is found in the composite hydrogels by scanning electron microscopy (SEM), and the pore size and the swelling ratio in NaCl solution decrease by the addition of HNTs and the immersing of ethanol. Chitosan/HNTs composite hydrogels show low cytotoxicity towards MC3T3-E1 cells. Also, the composite hydrogels show a maximum drug entrapment efficiency of 45.7% for doxorubicin (DOX) which is much higher than that of pure chitosan hydrogel (27.5%). All the results illustrate that the chitosan/HNTs composite hydrogels show promising applications as biomaterials.

1. Introduction

Recently, polysaccharide-based hydrogels have been widely recognized as biomaterials due to their excellent biocompatibility, bioactivity, and biodegradability, etc (Luo & Shoichet, 2004; Shimamoto et al., 2012; Shoichet, 2009). The typical application of the polysaccharide hydrogels includes drug delivery system, tissue engineering scaffold, wound dressing materials, prospective materials for soft tissue replacement, and antibacterial devices. Chitosan, derived from chitin deacetylation, is the second largest class of natural polysaccharides (Meibom et al., 2004). Chitosan can be easily dissolved in dilute acid solution and has potential application value in various fields such as water treatment, food industry, catalysis, agriculture and biomedicine (Bhattarai, Gunn, & Zhang, 2010; Ladet, David, & Domard, 2008; Zhang, Tao, Li, & Wei, 2011b). However, chitosan hydrogel film prepared via dissolving in acid solution and then sinking into the alkali solution always causes the degradation of chitosan macromolecule chains. This further leads to the decrease in the mechanical strength of chitosan hydrogel film. To overcome the shortcoming, several methods have been used to enhance their mechanical strength such as chemical cross-linking, nano-filler reinforcement (e.g. nanoclays, silica nanoparticles, carbon nanotubes and graphene), and blending with other polymers (Chatterjee, Lee, & Woo, 2009; Chen et al., 2017; Chen, Chen, Bai, & Li, 2013; Copello, Mebert, Raineri, Pesenti, & Diaz, 2011; H. Liu, Liu, Chen, & Liu, 2008; Spagnol et al., 2012; Xin et al., 2017; Zhang, Qadeer, & Chen, 2011a). Chemical cross-linking method has some drawbacks mainly due to the cytotoxicity and the brittleness brought by the cross-linking agents (Maggi, Ciccarelli, Diociaiuti, Casciardi, & Masci, 2011; Mi, Kuan, Shyu, Lee, & Chang, 2000). Fortunately, the chitosan molecules can be dissolved in lithium hydroxide/potassium hydroxide/urea composite solution through freezing–thawing process. Urea can destroy the hydrogen bonds among chitosan molecules and form a new hydrogen bond between chitosan and it. As a result, many forms of chitosan materials, such as hydrogel, film, aerogel, fiber, and plastic, can be fabricated by treatment of the alkali chitosan solution. For example, the compression fracture stress of the chitosan hydrogels constructed from their alkaline solution was nearly 100 times that of the chitosan hydrogels prepared by the traditional acid dissolving method and exhibit excellent biocompatibility as well as controlled drug release behavior (Duan, Liang, Cao, Wang, & Zhang,

* Corresponding author.
E-mail address: liumx@jnu.edu.cn (M. Liu).

http://dx.doi.org/10.1016/j.carbpol.2017.08.039
Received 3 June 2017; Received in revised form 25 July 2017; Accepted 9 August 2017
Available online 14 August 2017

2015). Also, tough and cell-compatible chitosan hydrogels prepared by first dissolving chitin in NaOH/urea solution and then deacetylation can be used as scaffolds for mouse bone mesenchymal stem cells, which shows promising applications such as stem cell research, cell therapy, and tissue engineering (Ding et al., 2016). Chitosan microspheres crosslinked by genipin were also prepared from chitosan solution in an alkali/urea aqueous system as multifunctional adsorbents for deproteinization and decoloration (Wei, Duan, Xu, & Zhang, 2017). However, the preparation of high-strength chitosan hydrogel for practical applications is still challenging.

Nanoparticles usually are used to reinforce polymer hydrogels due to the advantages including high strength, high stability, low cost, and abundant functions. A number of studies have been carried out in which different nanoparticles have been added to chitosan to enhance the mechanical, thermal, and biological properties. The nanopartciles include oxidized graphite, carbon nanotubes (CNTs), nano-carbon black, nano-hydroxyapatite, and nano-clay and so on (Darder, Colilla, & Ruiz-Hitzky, 2003; Wang, Shen, Zhang, & Tong, 2005). Clay is a fine-grained natural rock or soil material that combines many advantages such as naturally occurring materials, unique structure, good biocompatibility, and low cost. Addition of nanoclay can effectively improve the mechanical strength, antibacterial activity, and drug loading performance of chitosan (Deng et al., 2011; Deng et al., 2012; Jiang et al., 2015; Xu et al., 2012). Among the various clays, halloysite nanotubes (HNTs) represent a novel natural nanoparticle with unique structure and properties. HNTs have a similar chemical formula with kaolinite ($Al_2Si_2O_5(OH)_4{\cdot}nH_2O$), which show a unique empty tubular microstructure (Cai et al., 2012; Liu, Jia, Jia, & Zhou, 2014; Luo et al., 2010). HNTs show a high aspect ratio and high mechanical properties as well as good dispersion ability in polymer, so they are incorporated into different polymers to increase the hydrogel strength. The siloxanes and hydroxyl groups on HNTs surface can form hydrogen bonds with the polar groups of polymer matrix, which contributes to the enhancement of the mechanical properties (Huang, Liu, Long, Shen, & Zhou, 2017; Huang, Liu, & Zhou, 2017; Liu, Guo, Du, Chen, & Jia, 2009; Liu, Guo, Lei, Du & Jia Liu, Wu, Jiao, Xiong, & Zhou, 2013; Salam, Dong, & Davies, 2015). Recently, HNTs are used as drug delivery carriers for curcumin, doxorubicin (DOX), DNA, protein, and antibacterial agents (Lee, Jung, Cho, Geckeler, & Fuchs, 2013; Lvov, Wang, Zhang, & Fakhrullin, 2016; Yang et al., 2016). HNTs also can be applied in high-performance tissue engineering scaffolds, cancer early diagnose, and wound dressing materials (He, Liu, Shen, Long, & Zhou, 2017; Naumenko, Guryanov, Yendluri, Lvov, & Fakhrullin, 2016; Sandri et al., 2017). The advantages of HNTs for application in bicentennials include high adsorption ability, non-toxicity, good biocompatibility, good dispersion ability, and inexpensive. Previously, HNTs were added to cellulose NaOH/urea solution to prepare composite hydrogels using epichlorhydrine crosslinking. Compressive mechanical properties and drug delivery properties of cellulose composite hydrogels were significantly improved compared with pure cellulose hydrogel (Huang, Liu, Zhou, 2017). Also, the HNTs have been included into chitosan to form composites in terms of capsules, films, hydrogel beads, or porous scaffold or nanocomposite structures (Chiew et al., 2014; De Silva, Pasbakhsh, Goh, Chai, & Ismail, 2013; Govindasamy, Fernandopulle, Pasbakhsh, & Goh, 2014; Liu et al., 2016; Liu et al., 2013; Liu, Zhang, Wu, Xiong, & Zhou, 2012; Peng, Liu, Zheng, & Zhou, 2015). For example, Pasbakhsh et al. found that the addition of HNTs into chitosan could improve the tensile strength and thermal stability of chitosan membranes (De Silva et al., 2013). On the basis of the previous work, this work aims to incorporate HNTs into chitosan for preparing high-strength composite hydrogel and investigating the influence of the addition of HNTs on the properties of chitosan hydrogels. The chitosan/HNTs composite hydrogels are expected to be used as cellular scaffolds, drug delivery carrier, and wound healing materials.

Here, chitosan composite hydrogels reinforced with HNTs are prepared by heat treatment of the lithium hydroxide/potassium hydroxide/urea composite solution at 60 °C for 8 h and then regeneration in ethanol solution. Immersing in an aqueous ethanol solution with a different concentration (from 0 to 100 wt%) was used to allow for the formation of chain entanglements among the chitosan chains, which can significantly enhance the mechanical property of the chitosan hydrogel (Zhao et al., 2016). The effects of HNTs content and ethanol solution concentration on the physical and mechanical properties of composite hydrogels were investigated. HNTs show excellent reinforcing ability towards chitosan hydrogel. The biocompatibility of the composite hydrogels was further investigated by culturing the MC3T3-E1 cells. Furthermore, the drug loading property of composite hydrogels for doxorubicin (DOX) was investigated via physical adsorption. All the results show that the chitosan/HNTs composite hydrogel show promising applications as drug delivery carrier and wound healing dressing.

2. Experimental

2.1. Materials

Chitosan (CS) was supplied by Jinan Haidebei Marine Bioengineering Co. Ltd, China. The deacetylation and viscosity-average molecular weight were 95% and 600,000 g/mol respectively. The halloysite was acquired from Guangzhou Runwo Materials Technology Co., Ltd, China. Ultrapure water from a Milli-Q water system was used in all experiments. 4′,6-diamidino-2-phenylindole (DAPI) were purchased from Guangzhou Jetway Biotech Co., Ltd, China. Doxorubicin hydrochloride (DOX) was purchased from Nanjing Oddfoni Biological Technology Co. Ltd, China. LiOH, KOH, urea, and other chemicals reagents were purchased from Aladdin (Shanghai, China) were analytically pure without further purification.

2.2. Preparation of chitosan/HNTs composite hydrogels

The chitosan powder was dissolved and dispersed in 4.5 wt.% LiOH, 7.5 wt.% KOH and 8.5 wt.% urea composite solution according to the literature method (Duan et al., 2015). Subsequently, the dispersion was placed in −70 °C refrigerator to frozen overnight. The dispersion was then thawed and stirred at 20 °C to form a clear and transparent of chitosan solution with different concentration (1 wt.%, 2 wt.%, 3 wt.%, 4 wt.%, 5 wt.%). Then chitosan solution was centrifuged at 7000 rpm for 15 min at 5 °C to remove bubbles. Afterwards, the chitosan solution was cast into a cylindrical glass or plastic models and heated in 60 °C for 8 h to form physical hydrogel. The chitosan/HNTs composite hydrogel was prepared by adding HNTs powder into clear chitosan solution and stirring them at room temperature for 30 min to get a series of chitosan/HNTs composite solution. The weight ratio of HNTs to chitosan was 2: 1, 1: 1, 1: 2, and the corresponding code the composite hydrogels was CS2N1, CS1N1, CS1N2, respectively (Table 1). The

Table 1
Chitosan/HNTs composite hydrogels formulation and nomenclature.

Hydrogels	Chitosan content (g/100 mL)	HNTs content (g/100 mL)	HNTs percent (%)	Ethanol concentration (%)
2% CS	2	0	0	0
4% CS	4	0	0	0
5% CS	5	0	0	0
CS	3	0	0	0
CS2N1	3	1.5	33.3	0
CS1N1	3	3	50	0
CS1N2	3	6	66.6	0
CS/75%	3	0	0	75
CS2N1/75%	3	1.5	33.3	75
CS1N1/75%	3	3	50	75
CS1N2/75%	3	6	66.6	75

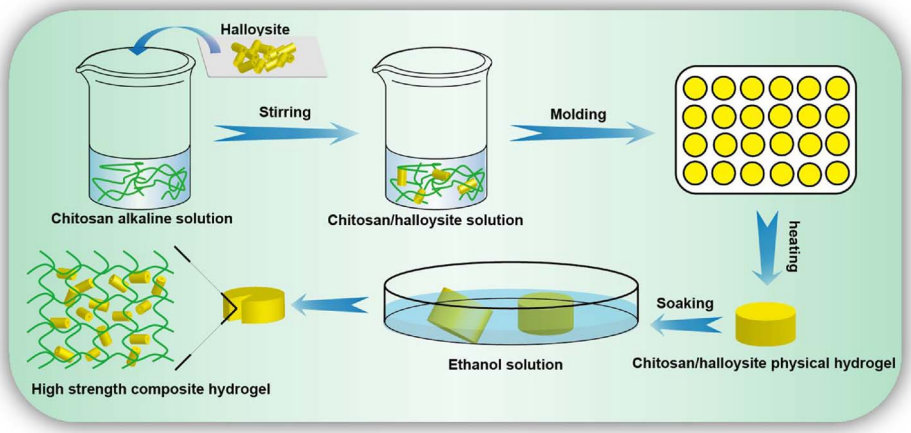

Fig. 1. Schematic illustrating the preparation process of the chitosan/HNTs composite hydrogels.

hydrogel code of 2% CS, 4% CS, and 5% CS meant the hydrogel was prepared from corresponding chitosan solution with concentration of 2 wt.%, 3 wt.%, and 5 wt.% respectively. All the hydrogels were taken out from the mold and thoroughly washed with deionized water to remove residual alkali/urea. The hydrogels were then immersed in different concentrations of ethanol solution (25%, 50%, 75%, 100%) at 5 °C for 3 days to prepare a series of high strength hydrogels (Fig. 1).

2.3. Characterization

The morphology of HNTs was observed with a LEO1530 VP SEM machine and a Philips Tecnai 12 TEM. Particle size distribution of HNTs in aqueous dispersion was conducted with a laser particle sizer (Beckman Coulter LS13 320). The dynamic light scattering (DLS) techniques was used to determine the hydrodynamic diameter. A rotated rheometer (Kinexus pro+, Malvern Instruments, Malvern, UK.) was used to measure the dynamic viscosity of the chitosan and chitosan/HNTs mixed solutions at the room temperature with the shear rate of 0.1 ~ 100 s^{-1}. Compressive property testing of the hydrogels was carried out using universal testing machine (UTM-1422, Chengde jinjian testing instrument, China) under 25 °C at a speed of 2 mm/min. The stress–strain curves for compressive–recovery of the hydrogels were obtained by compressing the samples to 10%, 20%, 30%, 40%, 50%, 60%, 70% strain and then reverting at a same speed (2 mm/min). The hysteresis in the stress–strain curve was recorded by the software. The section morphology of the hydrogels was analyzed by means of SEM (S-4800 FE, Hitachi) at voltage of 2 kV. Before observation, the wet hydrogels were freeze–dried, sectioned, and sputtered with a layer of gold. X-Ray Diffraction (XRD) profiles for lyophilized and milled hydrogel samples were generated using X-ray diffractometer (D8, Bruker) at room temperature. The scanning angle was from 5° to 60° and a scanning speed of 10°/min with 40 kV voltages and 15 mA current. The hydrogel powder samples were also analyzed using FT-IR spectrometer (VERTEX 70, Bruker) at room temperature from 400 cm^{-1} to 4000 cm^{-1}. The storage modulus of the hydrogels was analyzed in room temperature with strains sweep (0.1 ~ 10%) and frequency sweep (0.1 Hz ~ 100 Hz) for chitosan and chitosan/HNTs hydrogels with a sample diameter of 15 mm and a thickness of 1 mm by a rotated rheometer (Kinexus pro+, Malvern Instruments, Malvern, UK.). The strain sweep was conducted at a fixed frequency of 1 Hz, and the frequency sweep was conducted at a fixed strain of 0.5%. Water content of hydrogel samples was measured by placing 1 cm thick hydrogel film in moisture analyzer tray (MS-70, A & D's Moisture Analyzers, Japan) at 130 °C high temperature. The swelling behavior of the hydrogels was measured at 37 °C in NaCl solution (0.1 mol/L) and the equilibrium swelling rate (ESR) was calculated according to the following formula:

$$ESR = (W_s - W_d)/W_d \times 100\%$$

where, W_s and W_d was the weight the swollen hydrogels and the oven-dried hydrogels, respectively. All experiments were repeated over three times.

2.4. Cell viability

Mouse osteoblastic cells (MC3T3-E1) were cultured in DMEM supplemented with 10% FBS and 1% penicillin/streptomycin in a humidified atmosphere containing 5% CO_2. The hydrogel samples were swollen in sterile water to remove excess ethanol and then cut into films to be sterilized using high-pressure steam sterilization method. MC3T3-E1 cells were seeded on hydrogel samples with a density of 5.0×10^4 cells/well and cultured in constant temperature incubator. The cells on the material were subsequently stained with DAPI and then observed under fluorescence microscopy. For MTT assay, MC3T3-E1 cells were seeded onto hydrogel samples with a density of 5.0×10^4 cells/well in 24-well plate. 0.5% MTT solution was added to the wells at 1 day, 3 days and 5 days, and the cells culture was stopped after incubation for 4 h. The original culture medium was aspirated from 24-well plate and dimethyl sulfoxide was added to sufficiently dissolve the crystals. The OD value of each well was measured at 490 nm using a microplate reader.

2.5. DOX loading

CS, CS2N1, and CS1N2 hydrogels with a thickness of 1 mm were vacuum dried at 60 °C for 24 h to remove residual moisture. Then the dried hydrogel was soaked in DOX aqueous solution with concentration of 200 μg/mL in dark for 36 h at 37 °C. The determination of drug loading content and entrapment efficiency of hydrogels was based on a standard curve method using the formula.

$$\text{Drug loading content} = (W_{total} - W_{remain})/W_{sample} \times 100\%$$

$$\text{Entrapment efficiency (EE)} = (W_{total} - W_{remain})/W_{total} \times 100\%$$

Where, W_{total}, W_{remain}, and W_{sample} represent the initial DOX content, the amount of the remained DOX in the solution, and the total mass of hydrogel sample after drug-loading, respectively. The excitation wavelength of DOX was set as 480 nm.

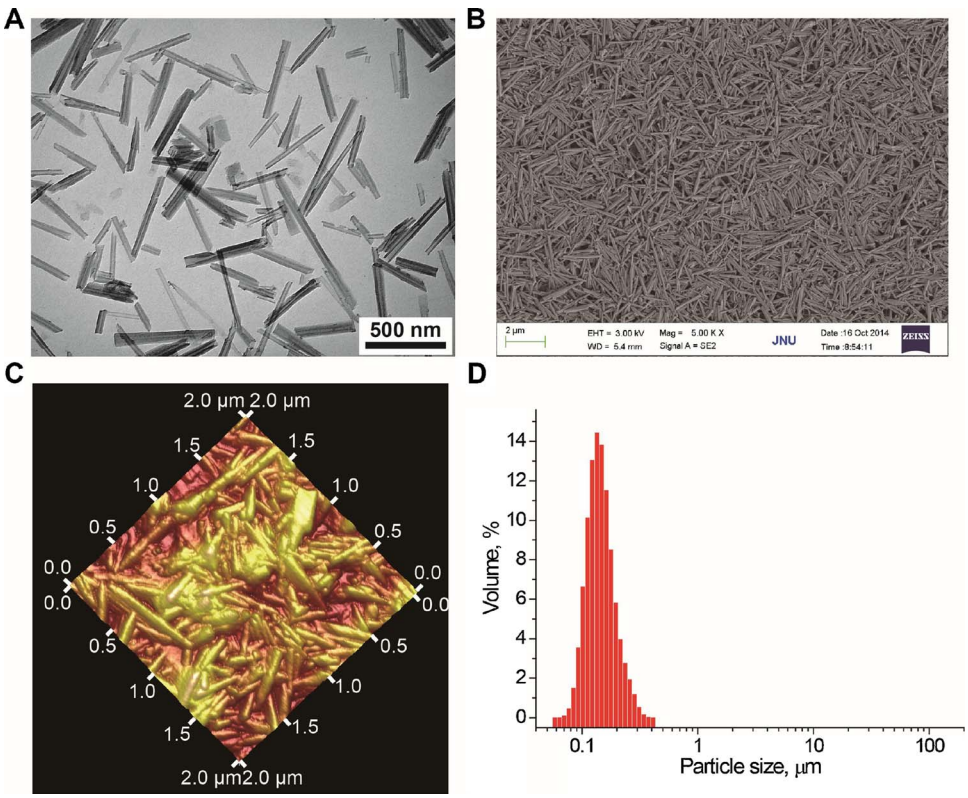

Fig. 2. Morphology and size distribution of the used HNTs: (A) TEM images; (B) SEM images; (C) AFM images; (D) DLS particle size distribution.

3. Results and discussion

3.1. Characterization of the used HNTs

HNTs are novel tubular like nanoparticles which derived from nature clay sources. The typical features of HNTs used as nanofillers of polymers include high aspect ratio, good dispersion ability, high adsorption performance, good biocompatibility, and low cost. Fig. 2 shows the TEM, SEM, and AFM images of the HNTs. From TEM image, one can see that HNTs exhibit long tubular like morphology with empty lumen inside. The length, outer diameter, and inner diameter of HNTs are in the range of 100 ~ 1000 nm, 25 ~ 60 nm, 15 ~ 30 nm, respectively. Although the dimension of the tubes is different, no HNTs aggregate is found in the TEM image. The aspect ratio of the HNTs is in the range of 4 ~ 20. The morphology of HNTs from SEM and AFM images agrees with the TEM result. Fig. 2(D) shows the DLS particle size distribution of HNTs in aqueous solution. The mean particle size of HNTs is 143 nm and their size ranges from 50 to 400 nm. All these data suggest that HNTs have unique structure and have high dispersion ability in aqueous systems, which can be potentially used as reinforcing agent for chitosan hydrogel.

3.2. Mechanical properties of chitosan/HNTs composite hydrogel

Mechanical properties of chitosan physical hydrogels prepared with different chitosan concentrations were first studied. As showed in Fig. 3(A), hydrogel compressive strength improves from 0.04 MPa (2% CS) to 0.14 MPa (5% CS) with the increase of chitosan concentration. The chitosan solution at 1% concentration cannot form physical hydrogel owing to the relatively low polymer content. However, the increase of compressive strength is accompanied by the decrease of fracture toughness for all hydrogel samples. 2% CS hydrogel can endure 60% deformation and keep the structure stable, while 5% CS hydrogel can only bear 47% deformation. From the mechanical testing result, the mechanical strength of 3% CS hydrogel is higher than that of 2% CS, and the fracture deformation is higher than that of 4% CS and 5% CS. Also, excessive chitosan concentration leads to too thick of the solution to mix with HNTs. Therefore, 3% concentration of chitosan solution is selected to prepare chitosan/HNTs composite hydrogels in the following section.

Fig. 3(B) shows the compressive stress-strain curve of chitosan/HNTs physical hydrogels. With the increase of HNTs content, the strength of composite hydrogel increases. This demonstrates a good reinforcing ability of the tubular HNTs towards chitosan. However, overall strength (0.058 ~ 0.104 MPa) of the hydrogels is low owing to the relatively less macromolecule chains entanglement. Therefore, the hydrogels were treated with ethanol solution with different concentration to further increase the strength. Fig. 3(C–F) further shows the compressive stress-strain curves of chitosan/HNTs composite hydrogels which were soaked in ethanol solution with different concentrations. It can be observed in the figures that the hydrogel strength and toughness increases with the increase of the ethanol concentration. The maximum compressive strength of the composite hydrogels is 0.86 MPa which is achieved by immersing the CS1N1 hydrogels in 100% ethanol. The compressive strength of the present chitosan/HNTs composite hydrogel is super than some of previously reported ones. For example, the carboxymethyl chitosan/gelatin/nanosilver composite hydrogels exhibited maximum compressive strength of 0.32 MPa (Zhou et al., 2012). Chitosan/polyvinyl alcohol (molar ratio = 1/15) hydrogel showed maximum compressive strength of 0.20 MPa (Wang, Turhan, & Gunasekaran, 2004). However, the chitosan/HNTs composite hydrogels are relatively weak compared with the recently reported epichlorohydrin cross-linked chitosan/rectorite/cellulose composites hydrogels (Tu et al., 2017). When ethanol concentration is higher than 75%, the fracture deformation of hydrogels decreases for all the groups (Fig. 3(F)). This can attribute to the decrease in brittleness by the excess chains entanglements. At a high ethanol concentration, the chitosan chains are rapidly and completely neutralized by ethanol, which leads to a high physical cross-linking density of the hydrogel. In contrast, at low ethanol concentrations, the hydrophobic interactions and chain

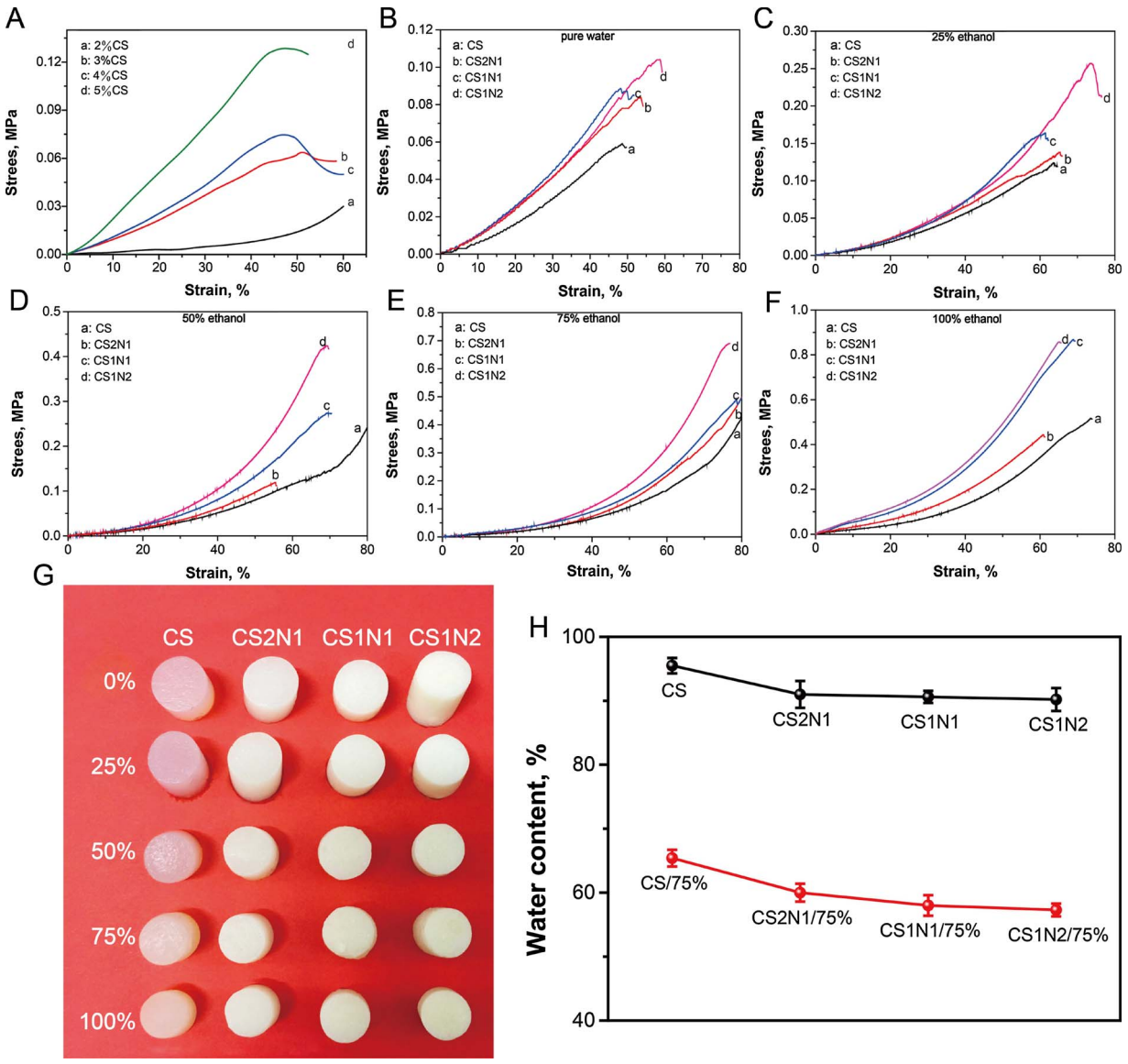

Fig. 3. (A) Compressive stress-strain curve of chitosan hydrogels with different chitosan solution concentrations; (B-F) Compressive stress-strain curve of chitosan/HNTs composite hydrogels soaked in different concentrations ethanol solution for 3 days, the ethanol solution concentrations are 0%, 25%, 50%, 75%, 100% respectively; (G) The appearance of chitosan/HNTs composite hydrogels immersed in different concentrations of ethanol solution for 3 days, the percentage represents the ethanol concentration; (H) Water content of chitosan/HNTs composite hydrogel as prepared and those soaked in 75% ethanol solution.

entanglements between the chitosan chains are disrupted by the diffusion of water molecules, which affect the final physical cross-links density as well as the water content of the hydrogels (Zhao et al., 2016). Fig. 3(G) shows a series of photos of the new prepared hydrogels and the hydrogels immersed in ethanol solution for 3 days. It can be seen that the hydrogel samples are subjected to dehydration and volume shrinks with the increase of ethanol concentration. Fig. 3(H) shows the water content of pure chitosan and chitosan/HNTs composite hydrogel before and after immersing in ethanol. Before immersing, the water content of the hydrogels is above 90%. In contrast, the water content is lowered to 60 ~ 70% after soaking in the ethanol solution. The incorporation of HNTs leads to the decrease of the water content of the hydrogel, which suggests that the composite hydrogels contains less water than that of pure chitosan hydrogel. Decreased water content also results in decreased pore size after freeze-drying, which will be illustrated below.

The cyclic compression curve of the pure chitosan and chitosan/HNTs composite hydrogel is illustrated in Fig. 4. During the loading-unloading cycle, the compressive stress is returned to the original zero for each successive cycle. It can be seen from all hydrogel samples show good cyclic compressibility. For example, the CS1N2/75% hydrogel undergo 7 times compression cycles without breaking, and the compressive strength is 0.71 MPa with over 70% maximum deformation. CS1N2/75% hydrogel shows the most excellent cycle compression performance among the hydrogel samples. The weakest CS hydrogel is broken after bearing 5 compression cycles with a maximum deformation of 59% and compressive strength of 0.14 MPa. The experimental results further prove that the deformation recovery capacity and physical strength of the hydrogel are substantially improved after immersing in ethanol solution. It is considered that the water molecules escape from the composite hydrogel network in ethanol solution, which makes the hydrogel network denser and thereby the hydrogel strength is improved. Also, the compressive stress of CS1N2 (0.19 MPa) hydrogel is higher than that of CS hydrogel (0.14 MPa), which suggests that the compressive strength of chitosan hydrogel is increased by HNTs even without immersing of ethanol solution. The enhanced compressive strength of chitosan hydrogel is appreciated for their practical applications such as in wound dressing, since the compression can enhance

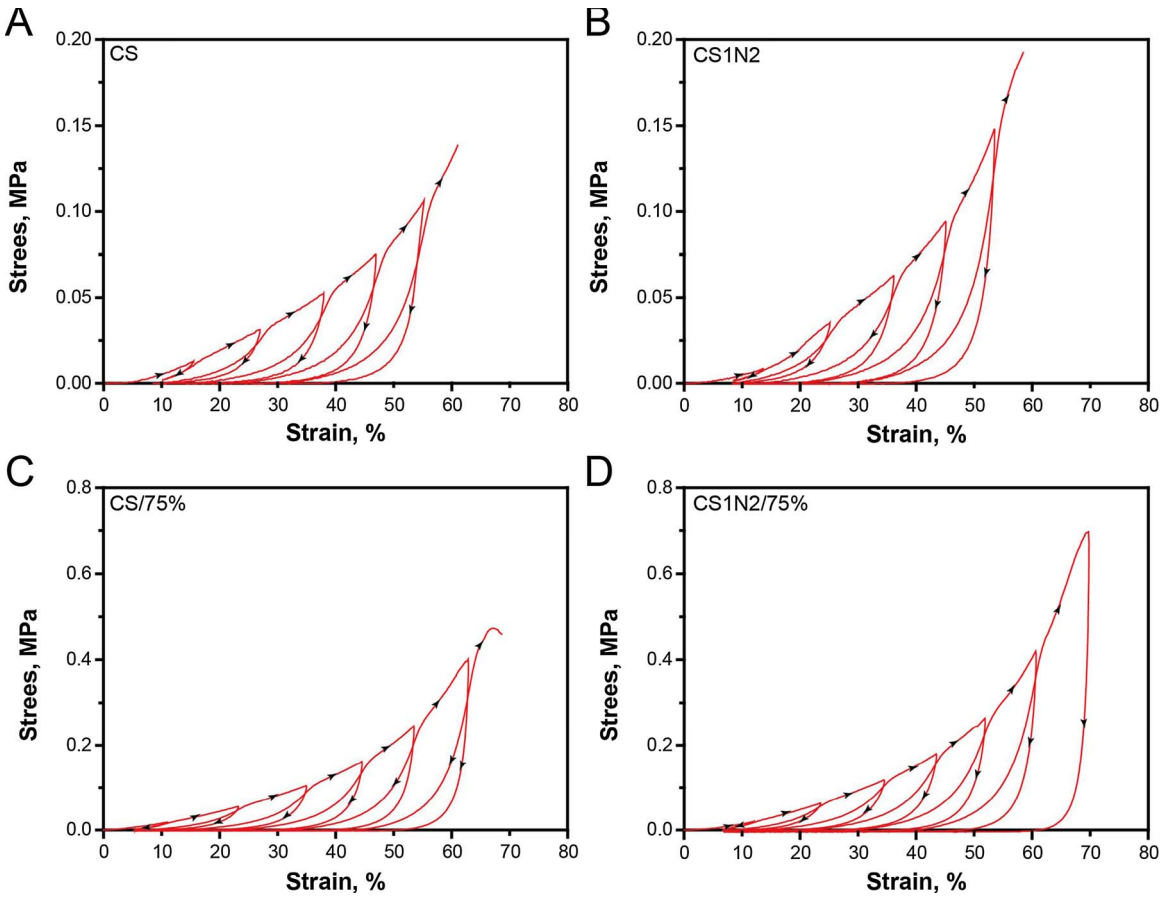

Fig. 4. Cycle compressive stress-strain curves of CS (A), CS1N2 (B), CS/75% (C), and CS1N2/75% (D).

liquid absorption around the wound sites and promote the wound healing process. Previous study suggested that the addition of HNTs indeed improved the hemostatic and wound healing property of chitosan (Liu, Shen et al., 2014). Although HNTs is not degradable in vivo, the good biocompatibility with very low toxicity makes HNTs safe in blood coagulation and wound healing applications (Alavi et al., 2014).

3.3. Rheological properties of chitosan/HNTs composite hydrogel

In order to further show the influence of HNTs on the structure of chitosan hydrogel, a serious of rheological properties of chitosan/HNTs composite hydrogel were determined. Firstly, the shear viscosity of the chitosan/HNTs composite solution was determined by rotating rheometer. As can be seen from Fig. 5**(A)**, the color of the chitosan composite solution becomes whiter with the increase of HNTs content. The original transparent state of pure chitosan solution turns into turbidity state for the composite solution. In addition, the shear viscosity of the solution is increased from 25 mPa of pure chitosan solution to 360 mPa of CS1N2 solution at a shear rate of 0.1 s^{-1}. The viscosity of the composite solution is decreased when the shear rate is raised, while the viscosity of the pure chitosan solution is almost unchanged. This may be because HNTs in the composite solution can form a loose network via interactions among them, and the network can be destroyed upon the increase in the shear rate. As a result, the viscosity of the composite solution is reduced significantly.

The shear modulus (G') curves of the composite hydrogels as a function of strain and frequency were studied in dynamic stress environment by rheometer. When the strain increases from 0.1% to 10% (Fig. 5(B)), the storage modulus (G') of the composite hydrogels increases with the increase of HNTs content. For example, G' of CS1N2 (597.4 Pa) at 1% strain is 2.22 times higher than that of pure chitosan hydrogel (185.5 Pa). The soaking in ethanol solution also has a reinforcing effect on the G' of hydrogel. The G' of CS2N1 composite hydrogels at 1% strain is increased from 548.9 Pa to 1272.5 Pa after soaking in ethanol solution. Fig. 5(B) further shows the G' curves at frequency sweep of the chitosan and chitosan/HNTs hydrogels. Consistent with the strain sweep, HNTs content and the ethanol solution are effective for the improvement of G' of the composite hydrogels. The G' of hydrogel samples after soaking in ethanol solution nearly keep constant in a frequency range from 0.1 ~ 10 Hz, indicating that the stiffness of composite hydrogels regenerated in ethanol solution is enhanced.

3.4. Structural characterization of chitosan/HNTs composite hydrogels

The effects of HNTs and ethanol solution on the chemical structure and crystal structure of chitosan were examined by FI-TR and XRD. As showed in Fig. 6(A), the broad absorption peaks of chitosan and chitosan/HNTs composite hydrogels at 3400–3500 cm^{-1} belong to the stretching vibration of hydroxyl groups of chitosan. The C═O absorption peak of chitosan appears at 1640 cm^{-1}(Ding et al., 2016; Kumirska et al., 2010). The characteristic peaks of HNTs at 3695, 3620, 1027, 910, 792 cm^{-1} are attributed to hydroxyl groups in the inner, hydroxyl groups in the outer surfaces, the Si–O–Si in-plane, the OH bending, the Al–OH bending vibrations of HNTs (Cheng, Yang, Liu, Zhang, & Frost, 2010). The chitosan/HNTs composite hydrogel mainly exhibit the IR peaks of HNTs expect the C—H bond peaks at 2820–2950 cm^{-1}, which is caused by the high HNTs content in the composites. The absorption peak of the hydroxyl group around 3450 cm^{-1} in the chitosan/HNTs composite hydrogels moves to higher wavenumber, which may be related to the presence of hydrogen bonds between chitosan and HNTs (Liu et al., 2013, 2012). After careful checking the spectra of the CS1N2

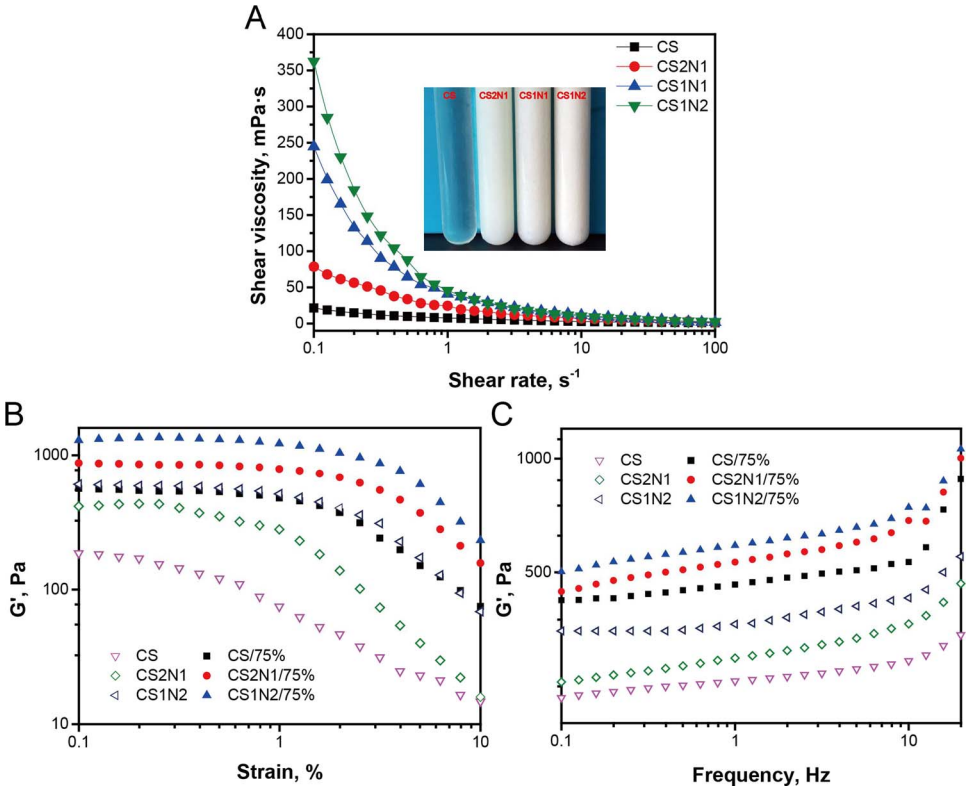

Fig. 5. Shear viscosity *vs* shear rate curves of pure chitosan and chitosan/HNTs composite hydrogels (A); The relationships between storage modulus (G') and strain (B) and frequency (C) for different hydrogel samples.

and CS1N2/75% hydrogel, one can be seen that the ethanol solution treatment has no effect on the IR activity of the chitosan/HNTs composite hydrogel.

Previous studied showed that pH value had a significant influence on the structural stability of HNTs in corrosive environments (Rachel, Dmitry, & Frank, 2012; Wang, Zhang, & Wang, 2013). For example, dissolution of the inner surface of HNTs was accompanied by the formation of $Al(OH)_3$ nanosheets in 1 mol dm^{-3} NaOH solution(Rachel et al., 2012). In the present work, alkali/urea mixture was used to dissolve chitosan and subsequently prepare composite hydrogels, so

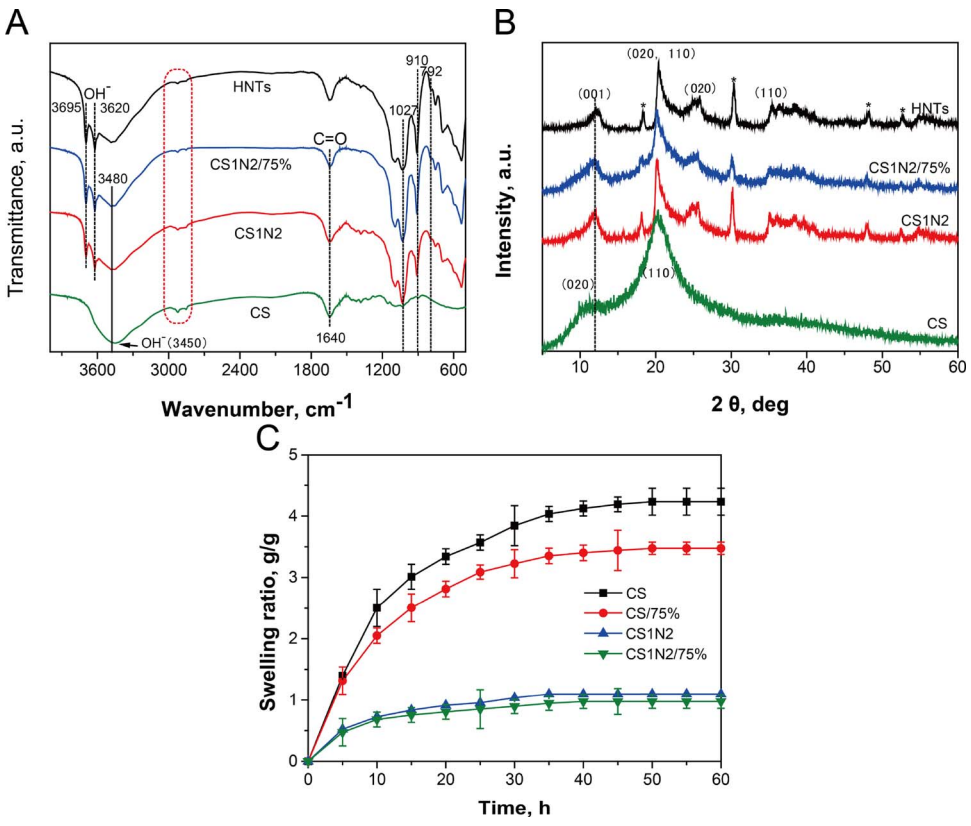

Fig. 6. FTIR spectra (A) and XRD patterns (B) of HNTs, chitosan, and chitosan/HNTs composites; (C) Swelling curves of hydrogel samples in NaCl solution at 37 °C.

XRD patterns were used to determine the crystal structure change of HNTs. The XRD curves of the hydrogel samples are shown in Fig. 6(B). Chitosan exhibits diffraction peaks nearby 12.8° and 20.8°, which are attributed to (020) and (110) planes of chitosan, respectively (Ogawa, Kimura, Wada, & Kuga, 2010; Tamura, Nagahama, & Tokura, 2006). The diffraction peaks of HNTs and chitosan/HNTs composites appear at 2θ = 11.7°, 20.1° and 24.7°, respectively, belonging to (001), (020,10) and (002) planes of HNTs. In addition, four peaks at 18, 30, 48, 53° appear in HNTs' XRD pattern due to the presence of some kaolinite and quartz powder dopants (mainly ferric oxide), which is agree with the results in literatures (Brindley, Robinson, & MacEwan, 1946; Rong et al., 2016). HNTs structure is preserved in the composite hydrogel, suggesting the alkali and urea in the chitosan solution have little effect on the structure of HNTs. Similarly, the XRD pattern of CS1N2 doesn't show the effect of ethanol solution on the composite hydrogel structure. Therefore, the chemical groups and crystal structure of composite hydrogels are unchanged after regeneration in ethanol solution.

The effect of HNTs on the swelling behavior of chitosan/HNTs hydrogels was evaluated by immersing them in NaCl solution (Fig. 6(C)). Before determination, the hydrogel samples were first dried in a vacuum oven at 60 °C for 24 h. And the dried hydrogel was placed in 0.1 M NaCl solution to achieve swelling equilibrium. The swelling ratio of pure chitosan hydrogel (4.2) is highest among the sample, which is about 6 times that of CS1N2 after 60 h. Compared with the hydrogel regenerated in ethanol solution, the swelling ratio of the hydrogel without soaking in ethanol solution is higher. This suggests that the increase of HNTs content and the regeneration in ethanol solution make the chitosan more contraction. As a result, the swelling ratio of hydrogels is decreased.

3.5. Cross-sectional morphology of chitosan/HNTs composite hydrogels

SEM images showing the pore structure of pure chitosan and chitosan/HNTs composite hydrogel were presented in Fig. 7. The pore size of the composite hydrogel changes in the range of 100 ~ 500 μm and becomes smaller and smaller as the HNTs content increases. It is found that the hydrogel pore size after regenerated in ethanol solution has the tendency to decrease. The pore size is about a half of that before regeneration, which is because the ethanol solution makes the hydrogels' skeleton contraction. Water molecules can enter the hydrogel matrix and hydrate the polar, hydrophilic groups of polymers, leading to 'primary bound water'. As the polar groups are hydrated, the network swells, and exposes hydrophobic groups, which also interact with water molecules, leading to hydrophobically-bound water, or 'secondary bound water'(Hoffman, 2002). On the other hand, the swelling of hydrogel in water is opposed by the covalent or physical crosslinks, leading to an elastic network retraction force. Thus, the hydrogel will reach an equilibrium swelling level. The water in hydrogel is assumed to fill the space between the network chains, and/or the center of larger pores, macropores or voids. During the freeze drying process, phase separation occurs and the water acts as porogenic agent in the hydrogel. Therefore, the addition of HNTs or soaking in ethanol solution of the chitosan hydrogels leads to the decrease in water content in the same volume hydrogels. As a result, the pore is smaller in the composite hydrogel compares with that in the pure chitosan hydrogel. The decrease of the pore size is benefit for the improvement of mechanical properties of composite hydrogel. The cross sections of chitosan/HNT composite hydrogels are further observed by fluorescence microscope by FITC-staining (Fig. 7(C)). Consistent with SEM results, both the pores exhibit interconnected structures with pore diameter in the range from 100 to 500 μm. The thickness of the pore walls is in ~20 μm. The addition of HNTs leads to a decrease of the pore size of chitosan hydrogels.

3.6. Cytotoxicity and drug loading of chitosan/HNTs composite hydrogels

In order to examine the biocompatibility of chitosan/HNTs composite hydrogels, the adhesion and growth behavior of cells on the hydrogel surface was observed. Fig. 8(A) shows the fluorescence microscopy of MC3T3-E1 cells cultured on hydrogel samples for 24 h and 72 h. The cell nucleis are stained with DAPI showing blue in the images. All samples show a good biocompatibility, and the blue area increase with the culture time increased from 24 h to 72 h, indicating the proliferation of cells on the hydrogel surface. Fig. 8(B) indicates the relative viability of cells cultured on the hydrogel surface by MTT assay. It can be seen that the cell viability for all groups is more than 70% (except CS1N2/75%) when the cells culture time is beyond five days, indicating the well proliferation of MC3T3-E1 cells on hydrogel surfaces. This suggests that the chitosan hydrogels regenerated in ethanol solution have excellent biocompatibility and with less cytotoxicity. The chitosan/HNTs composite hydrogels can serve as substrates for cell growth for application in tissue engineering or wound healing.

DOX is a chemotherapeutic agent for the cancers treatment such as breast cancer, bladder cancer, Kaposi's sarcoma, lymphoma and acute lymphoblastic leukemia (Ta, Dass, Larson, Choong, & Dunstan, 2009; Yang et al., 2016). Using DOX as the model drug, the drug loading

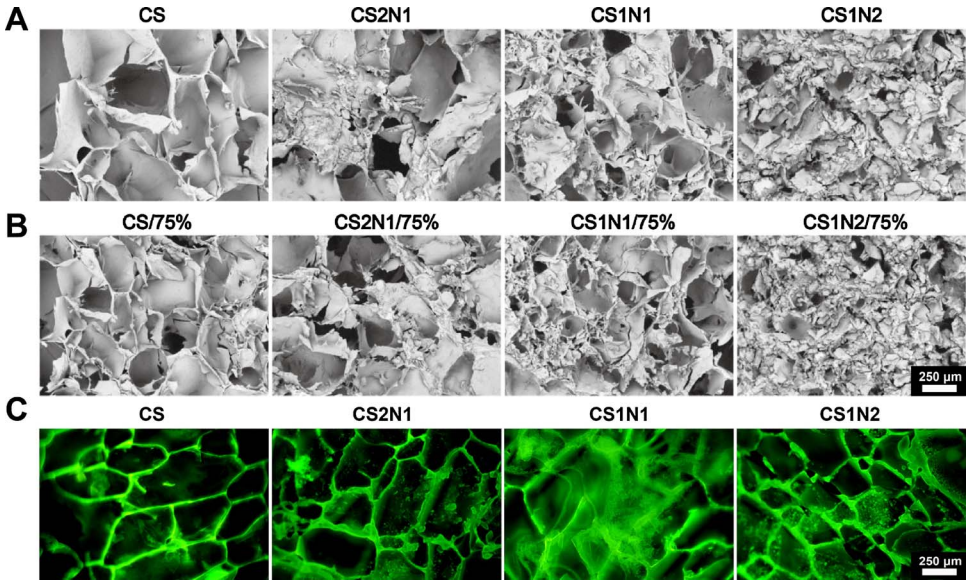

Fig. 7. The cross-section SEM images of pure chitosan and chitosan/HNTs composite hydrogels before (A) and after (B) immersing in 75% ethanol. Fluorescent images of cross section of pure chitosan and chitosan/HNTs composite hydrogels stained by FITC after immersing in 75% ethanol (C).

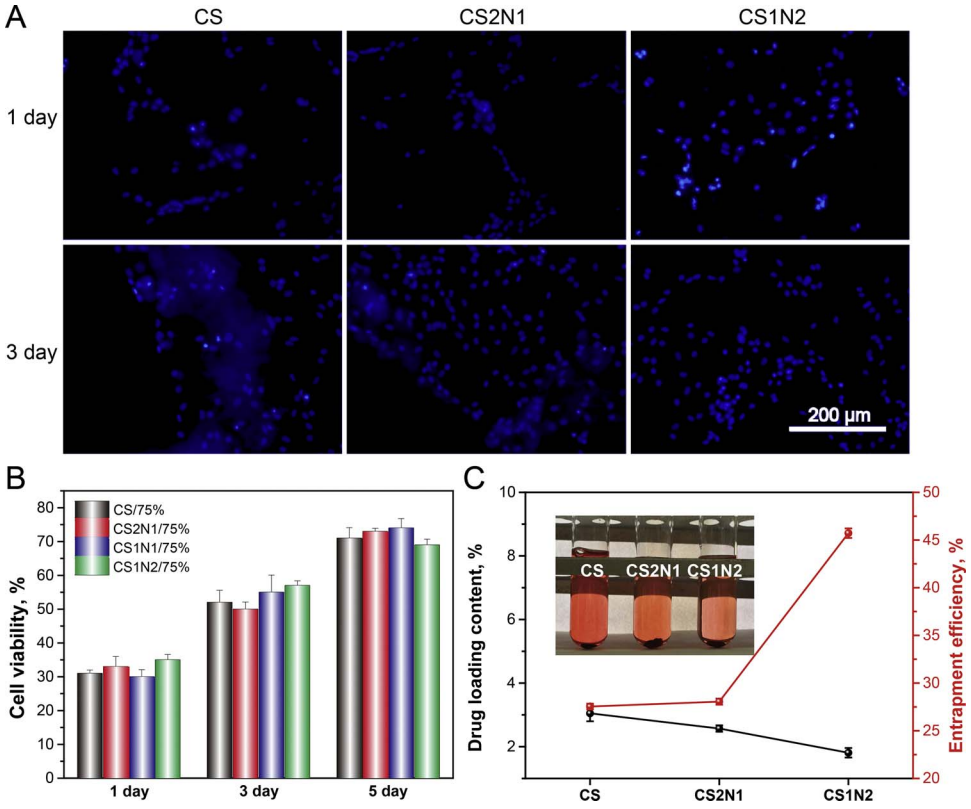

Fig. 8. (A) Fluorescent micrographs of MC3T3-E1 cells on the chitosan and chitosan/HNTs composite hydrogels (stained with DAPI); (B) The MC3T3-E1 cells relative viability on hydrogel samples by MTT assay; (C) The drug loading ability of CS, CS2N1 and CS1N2 hydrogel samples.

capacity of chitosan/HNTs physical hydrogels was studied by the adsorption of the drug by these hydrogels. As showed in inset of Fig. 8(C), DOX is successfully loaded into hydrogels with the same volume of drug solution. The color of the drug aqueous solution is getting lighter in the composite hydrogels samples compared with pure chitosan hydrogel. This suggests increased adsorption capacity of DOX by the addition of HNTs into chitosan. When the HNTs content in hydrogel is increased from 0% to 66.7%, the corresponding entrapment efficiency is increased from 27.5% to 45.7%. However, the drug loading content of composite hydrogel is less than that of pure CS hydrogel. Because of the synergistic effect of chitosan and HNTs and the high drug adsorption ability of both components, the drug entrapment ability is increased in the composite hydrogel. However, within the same volume hydrogel, the weight is increased in the composite hydrogels brought by HNTs, so the drug loading content in the composite hydrogels (calculated from the weight not from the volume) is therefore decreased. Compared to transparent pure CS hydrogel, the opaque composite hydrogels can prevent decomposition of loaded DOX in hydrogels. This suggests the chitosan/HNTs composite hydrogels have promising potential for application in drug loaded wound healing materials or tissue engineering scaffolds.

4. Conclusions

The 3% chitosan alkali/urea solution is selected to compound with HNTs for preparation composite hydrogels. To improve the hydrogel strength, the composite hydrogels is treated by heating at 60 °C and then soaking in ethanol solution. The viscosity of the composite solution increases with the increase of HNTs content. XRD and FT-IR show that the crystal and chemical structure of HNTs does not change in the composite hydrogels. The compressive strength and storage modulus determinations show that the addition of HNTs and the regeneration in ethanol leads to a significant increase in the mechanical properties and anti-deformation properties of the chitosan hydrogels. The composites hydrogel with 66.7% HNTs can undergo 7 times compression cycles without breaking with compressive strength of 0.71 MPa at 70% deformation, while pure chitosan hydrogel is broken after bearing 5 compression cycles with compressive strength of 0.14 MPa and a maximum deformation of 59%. The swelling capacity in NaCl solution and pore size of the composite hydrogel decrease by the addition of HNTs and the immersing of ethanol. The composite hydrogels have a good ability to support the growth of MC3T3-E1 cells, indicating their excellent biocompatibility. DOX loading ability of composite hydrogels is increased with the increase of HNTs content. All the experimental results demonstrate that the chitosan/HNTs composite hydrogels show promising potential in biomaterials such as drug loaded wound healing materials or tissue engineering scaffolds.

Acknowledgments

This work was financially supported by National High Technology Research and Development Program of China (2015AA020915), the National Natural Science Foundation of China (51473069 and 51502113), and the Guangdong Natural Science Funds for Distinguished Young Scholar (S2013050014606), Science and Technology Planning Project of Guangdong Province (2014A020217006), Guangdong Special support program (2014TQ01C127), the Pearl River S & T Nova Program of Guangzhou (201610010026), and Science and Technology Planning Project of Guangzhou (2017010160233).

References

Alavi, M., Totonchi, A., Okhovat, M. A., Motazedian, M., Rezaei, P., & Atefi, M. (2014). The effect of a new impregnated gauze containing bentonite and halloysite minerals on blood coagulation and wound healing. *Blood Coagulation & Fibrinolysis*, *25*(8), 856–859.

Bhattarai, N., Gunn, J., & Zhang, M. (2010). Chitosan-based hydrogels for controlled, localized drug delivery. *Advanced Drug Delivery Reviews*, *62*(1), 83–99.

Brindley, G., Robinson, K., & MacEwan, D. (1946). The clay minerals halloysite and meta-halloysite. *Nature*, *157*(3982), 225–226.

Cai, J., Liu, S., Feng, J., Kimura, S., Wada, M., Kuga, S., & Zhang, L. (2012).

Cellulose–silica nanocomposite aerogels by in situ formation of silica in cellulose gel. *Angewandte Chemie*, *124*(9), 2118–2121.
Chatterjee, S., Lee, M. W., & Woo, S. H. (2009). Enhanced mechanical strength of chitosan hydrogel beads by impregnation with carbon nanotubes. *Carbon*, *47*(12), 2933–2936.
Chen, Y., Chen, L., Bai, H., & Li, L. (2013). Graphene oxide–chitosan composite hydrogels as broad-spectrum adsorbents for water purification. *Journal of Materials Chemistry A*, *1*(6), 1992–2001.
Chen, J., Shi, X., Zhan, Y., Qiu, X., Du, Y., & Deng, H. (2017). Construction of horizontal stratum landform-like composite foams and their methyl orange adsorption capacity. *Applied Surface Science*, *397*, 133–143.
Cheng, H., Yang, J., Liu, Q., Zhang, J., & Frost, R. L. (2010). A spectroscopic comparison of selected Chinese kaolinite, coal bearing kaolinite and halloysite—A mid-infrared and near-infrared study. *Spectrochimica Acta Part A: Molecular and Biomolecular Spectroscopy*, *77*(4), 856–861.
Chiew, C. S. C., Poh, P. E., Pasbakhsh, P., Tey, B. T., Yeoh, H. K., & Chan, E. S. (2014). Physicochemical characterization of halloysite/alginate bionanocomposite hydrogel. *Applied Clay Science*, *101*, 444–454.
Copello, G. J., Mebert, A. M., Raineri, M., Pesenti, M. P., & Diaz, L. E. (2011). Removal of dyes from water using chitosan hydrogel/SiO 2 and chitin hydrogel/SiO 2 hybrid materials obtained by the sol?gel method. *Journal of Hazardous Materials*, *186*(1), 932–939.
Darder, M., Colilla, M., & Ruiz-Hitzky, E. (2003). Biopolymer- clay nanocomposites based on chitosan intercalated in montmorillonite. *Chemistry of Materials*, *15*(20), 3774–3780.
De Silva, R., Pasbakhsh, P., Goh, K., Chai, S.-P., & Ismail, H. (2013). Physico-chemical characterisation of chitosan/halloysite composite membranes. *Polymer Testing*, *32*(2), 265–271.
Deng, H., Li, X., Ding, B., Du, Y., Li, G., Yang, J., & Hu, X. (2011). Fabrication of polymer/layered silicate intercalated nanofibrous mats and their bacterial inhibition activity. *Carbohydrate Polymers*, *83*(2), 973–978.
Ding, B., Gao, H., Song, J., Li, Y., Zhang, L., Cao, X., ... Cai, J. (2016). Tough and cell-Compatible chitosan physical hydrogels for mouse bone mesenchymal stem cells in vitro. *ACS Applied Materials & Interfaces*, *8*(30), 19739–19746.
Duan, J., Liang, X., Cao, Y., Wang, S., & Zhang, L. (2015). High strength chitosan hydrogels with biocompatibility via new avenue based on constructing nanofibrous architecture. *Macromolecules*, *48*(8), 2706–2714.
Govindasamy, K., Fernandopulle, C., Pasbakhsh, P., & Goh, K. (2014). Synthesis and characterisation of electrospun chitosan membranes reinforced by halloysite nanotubes. *Journal of Mechanics in Medicine and Biology*, *14*(04), 1450058.
He, R., Liu, M., Shen, Y., Long, Z., & Zhou, C. (2017). Large-area assembly of halloysite nanotubes for enhancing the capture of tumor cells. *Journal of Materials Chemistry B*, *5*(9), 1712–1723.
Hoffman, A. S. (2002). Hydrogels for biomedical applications. *Advanced Drug Delivery Reviews*, *54*(1), 3–12.
Huang, B., Liu, M., Long, Z., Shen, Y., & Zhou, C. (2017). Effects of halloysite nanotubes on physical properties and cytocompatibility of alginate composite hydrogels. *Materials Science and Engineering: C*, *70*, 303–310.
Huang, B., Liu, M., & Zhou, C. (2017). Cellulose–halloysite nanotube composite hydrogels for curcumin delivery. *Cellulose*, *24*(7), 2861–2875.
Jiang, L., Lu, Y., Liu, X., Tu, H., Zhang, J., Shi, X., ... Du, Y. (2015). Layer-by-layer immobilization of quaternized carboxymethyl chitosan/organic rectorite and alginate onto nanofibrous mats and their antibacterial application. *Carbohydrate Polymers*, *121*, 428–435.
Kumirska, J., Czerwicka, M., Kaczyński, Z., Bychowska, A., Brzozowski, K., Thöming, J., & Stepnowski, P. (2010). Application of spectroscopic methods for structural analysis of chitin and chitosan. *Marine Drugs*, *8*(5), 1567–1636.
Ladet, S., David, L., & Domard, A. (2008). Multi-membrane hydrogels. *Nature*, *452*(7183), 76–79.
Lee, Y., Jung, G.-E., Cho, S. J., Geckeler, K. E., & Fuchs, H. (2013). Cellular interactions of doxorubicin-loaded DNA-modified halloysite nanotubes. *Nanoscale*, *5*(18), 8577–8585.
Liu, K.-H., Liu, T.-Y., Chen, S.-Y., & Liu, D.-M. (2008). Drug release behavior of chitosan–montmorillonite nanocomposite hydrogels following electrostimulation. *Acta Biomaterialia*, *4*(4), 1038–1045.
Liu, M., Guo, B., Du, M., Chen, F., & Jia, D. (2009). Halloysite nanotubes as a novel β-nucleating agent for isotactic polypropylene. *Polymer*, *50*(13), 3022–3030.
Liu, M., Guo, B., Lei, Y., Du, M., & Jia, D. (2009). Benzothiazole sulfide compatibilized polypropylene/halloysite nanotubes composites. *Applied Surface Science*, *255*(9), 4961–4969.
Liu, M., Zhang, Y., Wu, C., Xiong, S., & Zhou, C. (2012). Chitosan/halloysite nanotubes bionanocomposites: Structure, mechanical properties and biocompatibility. *International Journal of Biological Macromolecules*, *51*(4), 566–575.
Liu, M., Wu, C., Jiao, Y., Xiong, S., & Zhou, C. (2013). Chitosan–halloysite nanotubes nanocomposite scaffolds for tissue engineering. *Journal of Materials Chemistry B*, *1*(15), 2078–2089.
Liu, M., Jia, Z., Jia, D., & Zhou, C. (2014). Recent advance in research on halloysite nanotubes-polymer nanocomposite. *Progress in Polymer Science*, *39*(8), 1498–1525.
Liu, M., Shen, Y., Ao, P., Dai, L., Liu, Z., & Zhou, C. (2014). The improvement of hemostatic and wound healing property of chitosan by halloysite nanotubes. *RSC Advances*, *4*(45), 23540–23553.
Liu, M., Chang, Y., Yang, J., You, Y., He, R., Chen, T., & Zhou, C. (2016). Functionalized halloysite nanotube by chitosan grafting for drug delivery of curcumin to achieve enhanced anticancer efficacy. *Journal of Materials Chemistry B*, *4*(13), 2253–2263.
Luo, Y., & Shoichet, M. S. (2004). A photolabile hydrogel for guided three-dimensional cell growth and migration. *Nature Materials*, *3*(4), 249–253.
Luo, P., Zhao, Y., Zhang, B., Liu, J., Yang, Y., & Liu, J. (2010). Study on the adsorption of Neutral Red from aqueous solution onto halloysite nanotubes. *Water Research*, *44*(5), 1489–1497.
Lvov, Y., Wang, W., Zhang, L., & Fakhrullin, R. (2016). Halloysite clay nanotubes for loading and sustained release of functional compounds. *Advanced Materials*, *28*(6), 1227–1250.
Maggi, F., Ciccarelli, S., Diociaiuti, M., Casciardi, S., & Masci, G. (2011). Chitosan nanogels by template chemical cross-linking in polyion complex micelle nanoreactors. *Biomacromolecules*, *12*(10), 3499–3507.
Meibom, K. L., Li, X. B., Nielsen, A. T., Wu, C.-Y., Roseman, S., & Schoolnik, G. K. (2004). The Vibrio cholerae chitin utilization program. *Proceedings of the National Academy of Sciences of the United States of America*, *101*(8), 2524–2529.
Mi, F.-L., Kuan, C.-Y., Shyu, S.-S., Lee, S.-T., & Chang, S.-F. (2000). The study of gelation kinetics and chain-relaxation properties of glutaraldehyde-cross-linked chitosan gel and their effects on microspheres preparation and drug release. *Carbohydrate Polymers*, *41*(4), 389–396.
Naumenko, E. A., Guryanov, I. D., Yendluri, R., Lvov, Y. M., & Fakhrullin, R. F. (2016). Clay nanotube–biopolymer composite scaffolds for tissue engineering. *Nanoscale*, *8*(13), 7257–7271.
Ogawa, Y., Kimura, S., Wada, M., & Kuga, S. (2010). Crystal analysis and high-resolution imaging of microfibrillar α-chitin from Phaeocystis. *Journal of Structural Biology*, *171*(1), 111–116.
Peng, Q., Liu, M., Zheng, J., & Zhou, C. (2015). Adsorption of dyes in aqueous solutions by chitosan–halloysite nanotubes composite hydrogel beads. *Microporous and Mesoporous Materials*, *201*, 190–201.
Rachel, D. W., Dmitry, V. B., & Frank, C. W. (2012). The stability of halloysite nanotubes in acidic and alkaline aqueous suspensions. *Nanotechnology*, *23*(6), 065705.
Rong, R., Xu, X., Zhu, S., Li, B., Wang, X., & Tang, K. (2016). Facile preparation of homogeneous and length controllable halloysite nanotubes by ultrasonic scission and uniform viscosity centrifugation. *Chemical Engineering Journal*, *291*, 20–29.
Salam, H., Dong, Y., & Davies, I. (2015). *Development of bio-based polymer/clay nanocomposites: A critical review. Fillers and reinforcements for advanced nanocomposites*. UK: Woodhead Publishing, 101–132.
Sandri, G., Aguzzi, C., Rossi, S., Bonferoni, M. C., Bruni, G., Boselli, C., ... Caramella, C. (2017). Halloysite and chitosan oligosaccharide nanocomposite for wound healing. *Acta Biomaterialia*, *57*, 216–224.
Shimamoto, N., Tanaka, Y., Mitomo, H., Kawamura, R., Ijiro, K., Sasaki, K., & Osada, Y. (2012). Nanopattern fabrication of gold on hydrogels and application to tunable photonic crystal. *Advanced Materials*, *24*(38), 5243–5248.
Shoichet, M. S. (2009). Polymer scaffolds for biomaterials applications. *Macromolecules*, *43*(2), 581–591.
Spagnol, C., Rodrigues, F. H., Pereira, A. G., Fajardo, A. R., Rubira, A. F., & Muniz, E. C. (2012). Superabsorbent hydrogel composite made of cellulose nanofibrils and chitosan-graft-poly (acrylic acid). *Carbohydrate Polymers*, *87*(3), 2038–2045.
Ta, H. T., Dass, C. R., Larson, I., Choong, P. F., & Dunstan, D. E. (2009). A chitosan–dipotassium orthophosphate hydrogel for the delivery of Doxorubicin in the treatment of osteosarcoma. *Biomaterials*, *30*(21), 3605–3613.
Tamura, H., Nagahama, H., & Tokura, S. (2006). Preparation of chitin hydrogel under mild conditions. *Cellulose*, *13*(4), 357–364.
Tu, H., Yu, Y., Chen, J., Shi, X., Zhou, J., Deng, H., & Du, Y. (2017). Highly cost-effective and high-strength hydrogels as dye adsorbents from natural polymers: Chitosan and cellulose. *Polymer Chemistry*, *8*(19), 2913–2921.
Wang, T., Turhan, M., & Gunasekaran, S. (2004). Selected properties of pH-sensitive, biodegradable chitosan–poly(vinyl alcohol) hydrogel. *Polymer International*, *53*(7), 911–918.
Wang, S.-F., Shen, L., Zhang, W.-D., & Tong, Y.-J. (2005). Preparation and mechanical properties of chitosan/carbon nanotubes composites. *Biomacromolecules*, *6*(6), 3067–3072.
Wang, Q., Zhang, J., & Wang, A. (2013). Alkali activation of halloysite for adsorption and release of ofloxacin. *Applied Surface Science*, *287*, 54–61.
Wei, X., Duan, J., Xu, X., & Zhang, L. (2017). Highly efficient one-step purification of sulfate polysaccharides via chitosan microspheres adsorbents. *ACS Sustainable Chemistry & Engineering*, *5*(4), 3195–3203.
Xin, S., Zeng, Z., Zhou, X., Luo, W., Shi, X., Wang, Q., ... Du, Y. (2017). Recyclable Saccharomyces cerevisiae loaded nanofibrous mats with sandwich structure constructing via bio-electrospraying for heavy metal removal. *Journal of Hazardous Materials*, *324*, 365–372.
Xu, R., Xin, S., Zhou, X., Li, W., Cao, F., Feng, X., & Deng, H. (2012). Quaternized chitosan–organic rectorite intercalated composites based nanoparticles for protein controlled release. *International Journal of Pharmaceutics*, *438*(1), 258–265.
Yang, J., Wu, Y., Shen, Y., Zhou, C., Li, Y.-F., He, R.-R., & Liu, M. (2016). Enhanced therapeutic efficacy of doxorubicin for breast cancer using chitosan oligosaccharide-modified halloysite nanotubes. *ACS Applied Materials & Interfaces*, *8*(40), 26578–26590.
Zhang, H., Qadeer, A., & Chen, W. (2011a). In situ gelable interpenetrating double network hydrogel formulated from binary components: Thiolated chitosan and oxidized dextran. *Biomacromolecules*, *12*(5), 1428–1437.
Zhang, Y., Tao, L., Li, S., & Wei, Y. (2011b). Synthesis of multiresponsive and dynamic chitosan-based hydrogels for controlled release of bioactive molecules. *Biomacromolecules*, *12*(8), 2894–2901.
Zhao, D., Huang, J., Zhong, Y., Li, K., Zhang, L., & Cai, J. (2016). High-Strength and high-Toughness double-Cross-Linked cellulose hydrogels: A new strategy using sequential chemical and physical cross-Linking. *Advanced Functional Materials*, *26*(34), 6279–6287.
Zhou, Y., Zhao, Y., Wang, L., Xu, L., Zhai, M., & Wei, S. (2012). Radiation synthesis and characterization of nanosilver/gelatin/carboxymethyl chitosan hydrogel. *Radiation Physics and Chemistry*, *81*(5), 553–560.